Final Report

The Influence of Atmospheric Scattering on GLAS Altitude Measurements

UW 144-GP84
NASA NAS5-33015

E.W.Eloranta
Principal Investigator

University of Wisconsin
Space Science and Engineering Center
1225 W. Dayton St.
Madison,Wis
Tel (608)-262-7327

1 Abstract

The Geoscience Laser Altimeter System (GLAS) is designed to map Arctic and Antarctic ice topography. Propagation delays caused by atmospheric scattering from clouds and aerosols will introduce a bias in measured altitudes. Arctic stratus clouds, which are characterized by droplet diameters of $\sim$ 15 microns and altitudes of $\sim$ 1 km, produce the most significant errors. Even a very tenuous cloud with an optical depth of only 0.2 will decrease the apparent altitude of the surface by up to 20 cm. Errors produced by most cirrus, "diamond dust" ice crystal precipitation and arctic haze will be less than 1 cm.

2 Background

The GLAS altimeter will map surface topography by measuring the round trip flight time of photons from the satellite to the surface. When clouds and aerosols are present in the atmosphere, some of the photons will be forward scattered by particles without leaving the receiver field of view. These photons, which have been deflected from the straight line path to surface, will increase the average round-trip time of the observed pulse and thereby introduce errors in the measured altitude.

Clouds and aerosols are prevalent features of the Arctic and Antarctic. Walden and Warren, 1996, document the percentage of time various sky conditions are observed at the South Pole (table 1). Notice that only 21% of the summer days and 5% of the winter days are completely clear.

SEASON	CLR	CLRDD	SCT	BKN	OVC	BS
Summer	21	2	28	18	29	2
Autumn	14	7	28	16	30	5
Winter	5	14	29	10	27	15
Spring	12	5	39	17	32	4

Where: CLR = clear sky, CLRDD = ice crystals in clear sky, SCT = scattered cloud, BKN = broken clouds, OVC = overcast, and BS = blowing snow.

Table 1: Percentage of cloudy days at the South Pole as a function of season and cloud type.

Measurements in the arctic show a persistent, wide-spread haze. The optical depth varies with season, with maximum values during the winter and spring (Shaw, 1982, 1995; Meyer et al., 1991, Heber et al., 1996). Typical optical depths in the arctic haze vary between 0.02 and 0.08 at a wavelength of 1 micron.

Cloud cover climatologies for the arctic are mostly derived from visual surface observations at a few sites and are therefore quite subjective. The available statistics show low altitude stratus clouds covering much of the arctic with summertime cloud cover percentages as high as 90% and wintertime values in the 40% to 70% range (Curry et al. 1996).

Most GLAS altitude observations will be made in the presence of aerosol layers and/or clouds. Atmospheric scattering will increase the average path photon path length producing a bias in the measured altitudes. This report attempts to determine if these bias errors are likely to be significant and to estimate the potential bias in data acquired under representative high latitude cloud and aerosol conditions.

3 Derivation

In this section we derive expressions for the additional path delay accrued when a photon is scattered from an atmospheric particle before impacting on the surface. Figure 1 shows the scattering geometry. The GLAS lidar is located at an altitude, z_{orb}, above the surface. The lidar accepts photons from an angular field of view, η. A non-divergent laser is assumed.

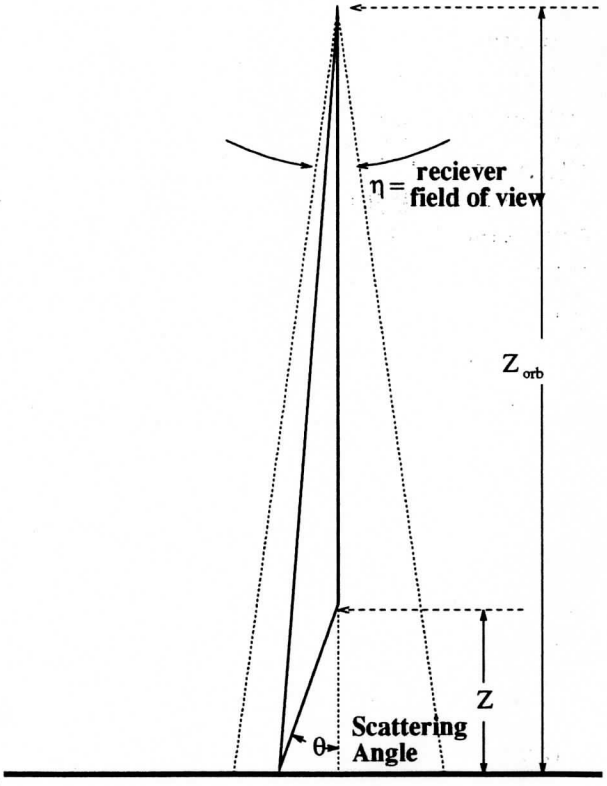

Figure 1: Scattering Geometry. The bold line shows the path of a photon which is scattered by an angle θ at an altitude z.

A photon scattered by an angle, θ, at altitude, z, above the surface will travel an extra distance, δ, before reaching the surface. (The same additional path is traveled by a photon which is first scattered from the surface at an angle near 180 degrees and then forward scattered toward the lidar by an angle, θ, at an altitude z.)

$$\delta = \frac{z}{cos(\theta)} - z \tag{1}$$

For small scattering angles $cos(\theta) \approx 1 - \theta^2/2$. Thus, equation 1 can be approximated by:

$$\delta = z\frac{\theta^2}{2}, \tag{2}$$

In order to calculate the mean path delay accrued by photons, the probability of scattering must be known as a function of angle. This requires an equation for the phase function, $\mathcal{P}$, as a function of the scattering angle θ. Diffraction theory shows that 1/2 of the energy scattered by particles which are large compared to the wavelength of the light is scattered into a narrow forward diffraction peak. A reasonable approximation to this forward scattering peak can be achieved with a Gaussian (see Eloranta, 1998). In this treatment we assume a phase function which is the sum of a Gaussian forward peak containing 1/2 of the scattered energy with the other half in an isotropic component. This phase function can be expressed as:

$$\frac{\mathcal{P}(\theta)}{4\pi} = \frac{1}{2\pi\theta_s^2} exp(-\frac{\theta^2}{\theta_s^2}) + 1/(8\pi), \tag{3}$$

To compute an average value of delta for all scattering events at altitude, z, we begin by substituting the expression for δ into equation 1 and integrating over all photon paths inside the receiver angular field of view, η, when the lidar is located at an altitude of z_{orb}. Note that $d\delta = z\theta d\theta$, and the maximum delay, δ_m, which can be accrued without losing the photon from the receiver field of view is:

$$\delta_m = z\left(\sqrt{(\frac{\eta^2 z_{orb}^2}{4z^2} + 1)} - 1\right), \tag{4}$$

For the proposed GLAS values, $\eta = 475\mu$rad and $z_{orb} = 600$ km, thus, the product $\eta z_{orb} =$ 285 m. Thus, except when z is less than $\sim$ 300 m, equation 4 can be expanded in a series and simplified to:

$$\delta_m = \frac{\eta^2 z_{orb}^2}{8z} \tag{5}$$

The average additional path length, $\overline{\delta_g}$, traveled by photons scattered in the Gaussian diffraction peak:

$$\overline{\delta_g} = \frac{\frac{1}{2\pi\theta_s^2}\int_0^{2\pi}\int_0^{\delta_m}\frac{\delta}{z}exp(-\frac{2\delta}{z\theta_s^2})d\delta d\phi}{\frac{1}{2\pi\theta_s^2}\int_0^{2\pi}\int_0^{\delta_m}\frac{1}{z}exp(-\frac{2\delta}{z\theta_s^2})d\delta d\phi} = \frac{\int_0^{\delta_m}\delta exp(-\frac{2\delta}{z\theta_s^2})d\delta}{\int_0^{\delta_m}exp(-\frac{2\delta}{z\theta_s^2})d\delta} \tag{6}$$

$$\overline{\delta_g} = \frac{z\theta_s^2}{2} - \frac{\delta_m exp(-\frac{2\delta_m}{z\theta_s^2})}{1 - exp(-\frac{2\delta_m}{z\theta_s^2})} \tag{7}$$

We now consider the average path delay, $\overline{\delta_i}$, accrued by the isotropic component of the scattering phase function $\frac{\mathcal{P}(\theta)}{4\pi} = \frac{1}{8\pi}$. Because the scattering is not restricted to small angles, as it was for the diffracted component, this computation does not use small angle approximations.

$$\overline{\delta_i} = \frac{z\int_0^{\theta_m}(\frac{1}{cos(\theta)} - 1)sin(\theta)d\theta}{(\int_0^{\theta_m} sin(\theta)d\theta} \tag{8}$$

$$= z\left(\frac{-log(cos(\theta_m)}{1 - cos(\theta_m)} - 1\right) \tag{9}$$

Where θ_m is the largest scattering angle which remains inside the reciever field of view when the photon is scattered at altitude, z.

$$\theta_m = atan(\frac{\eta z_{orb}}{2z}) \tag{10}$$

In order to compute the average delay of all photons which are detected we must compute a weighted average of the delays encountered by photons scattered in the diffraction peak and photons scattered isotropically by the atmosphere during the round trip to the surface scattering. Photons which have not encountered an atmospheric scattering must also be included in this average.

If S_1 is the GLAS lidar signal received from the earth's surface without the atmosphere, we expect attenuation to reduce the observed signal, S, to: $S = S_1 e^{-2\tau}$. Where τ is the optical depth of the atmospheric column. Because tmospheric absorption is small at the GLAS wavelength of 1.06 microns, attenuation is primarily due to the scattering of photons. However, as shown above, some of the scattered photons remain in the receiver field of view and thus contribute to the received signal. If none of the scattered photons were lost from the field of view, and the near backscatter surface reflectivity was isotropic, we could write the return signal as:

$$S = S_1 e^{-2\tau} e^{2\tau} \tag{11}$$

Expanding the last term in a power series yields:

$$S = S_1 e^{-2\tau}(1 + 2\tau + \frac{4\tau^2}{2}\cdots) \tag{12}$$

The terms of the expanded exponential can be readily identified as the relative contributions due to photons which have encountered successively larger numbers of atmospheric scatterings. The first term inside the parenthes of equation 12, is the relative contribution of photons which have not encounter an atmospheric scattering. The second term, 2τ, is the contribution due to photons which have encountered one atmospheric scattering and

the third term, $\frac{4\tau^2}{2}$, is the contribution due to photons which are scattered twice in the atmosphere.

Equation 12 overestimates the return signal because it does not account for photons that are scattered out of the receiver field of view. Examination of the geometry presented in figure 1 shows, that except for very small z, most of the photons scattered in the isotropic part of the phase function are lost from the field of view. Thus, only about 1/2 of the photons can contribute to the terms of the expanded exponential in equation 12. Considering only cases where the optical depth the of atmosphere is less than 1/2, and then reducing the value of τ in the exponential expansion by a factor of ~ 2 to account for the lost isotropically scattered photons, makes the third and higher order terms small. Equation 12 can then be approximated as:

$$S = S_1 e^{-2\tau}(1 + f_i\tau + f_g\tau) \tag{13}$$

Where the optical depth has been divided into separate equal components for the Gaussian and isotropic scattering events and the separate components have multiplied by the fraction of the photons, f_i and f_g, which remain in the receiver field of view for each type of atmospheric scattering. For a physically thin cloud located at an altitude z:

$$f_g = \frac{1}{\pi\theta_s^2}\int_0^{2\pi}\int_0^{\delta_m}\frac{1}{z}exp(-\frac{2\delta}{z\theta_s^2})d\delta d\phi = 1 - exp(-\frac{2\delta_m}{z\theta_s^2}) \tag{14}$$

$$f_i = \frac{1}{4\pi}\int_0^{2\pi}\int_0^{\theta_m} sin(\theta)d\theta d\phi = \frac{1}{2}(1 - cos(\theta_m)) \tag{15}$$

where δ_m and θ_m are given by equations 4 and 10, respectively. The average path delay accrued by all photons detected after passing through a physically thin cloud at altitude, z, can now be computed by substituting equations 7, 9, 14, and 15 into the following expression:

$$\overline{\delta_t} = \tau\frac{\overline{\delta_g}f_g + \overline{\delta_i}f_i}{1 + f_g\tau + f_i\tau}. \tag{16}$$

A comparison of the Gaussian phase diffraction peak described in equation 4 with rigorous diffraction theory shows that the parameter θ_s is a function of particle radius, r, and wavelength, λ. It can be approximated as follows:

$$\theta_s^2 \approx \frac{\lambda^2}{\pi^2 r^2}. \tag{17}$$

4 Computations

In this section we will estimate the possible effect of high latitude clouds and aerosols on GLAS altitude determinations. Cloud and aerosol observations from the literature are used to define likely values of particle size, cloud altitude and optical depth. The conditions selected are certain to be observed in some cases, they represent highly likely conditions: not worst case conditions. As in other parts of the world, a large variety of atmospheric particle

sizes and cloud optical depths are likely to exist in the Arctic and Antarctic. Relatively few measurements describing the optical properties of high latitude clouds and aerosols have been published and most of these are the result of short campaigns. Very few cloud observations are available above the high altitude ice sheets of Antarctica and Greenland.

Average increases in photon path length due to atmospheric scattering will be presented for physically thin clouds as a function of particle size and cloud altitude. For clouds, with a distribution of particle sizes and finite thickness, the particle radius should be interpreted as the effective radius (ie the third moment of the particle size divided by the second moment) and the results averaged over the the range of cloud altitudes weighted by the scattering cross section profile of the cloud.

4.1 Diamond Dust

Arctic observers frequently report the occurrence of ice crystal precipitation from clear skies. These "diamond dust" episodes will provide surface returns from the GLAS lidar. It is therefore important to access the influence of ice crystal scattering.

Smiley et al., 1980, report observing long lasting "diamond dust" episodes on 36 of 146 days of lidar profiling between March and November of 1975 at the South Pole. Ice crystals from 5 microns to 1 mm were observed, however those smaller than 50 microns could not be reliably separated from artifacts on their particle replicator. Thus, their published data does not attempt to describe the number of small crystals. They do not provide measurements of the optical depth. Representative vertical profiles measured with their lidar are included in the paper. An sample profile is shown in figure 2. A paper by Heber et al., 1996,

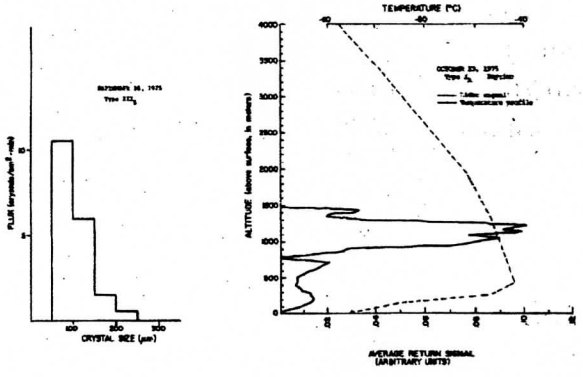

Figure 2: Examples of particle sizes and a lidar profile measured at the South Pole during the occurrence of "diamond dust" precipitation. (Smiley, 1980)

provides a climatology of optical depth measurements from Spitzbergen (fig. 3). They suggest that the Febuary values of optical depth are likely to include a strong component due to "diamond dust". Combining their February value of $\tau \sim 0.05$ with altitude and

particle size information from Smiley et al., 1989, allows us to access the probable effect of clear air ice crystal scattering on GLAS altitudes (fig. 4).

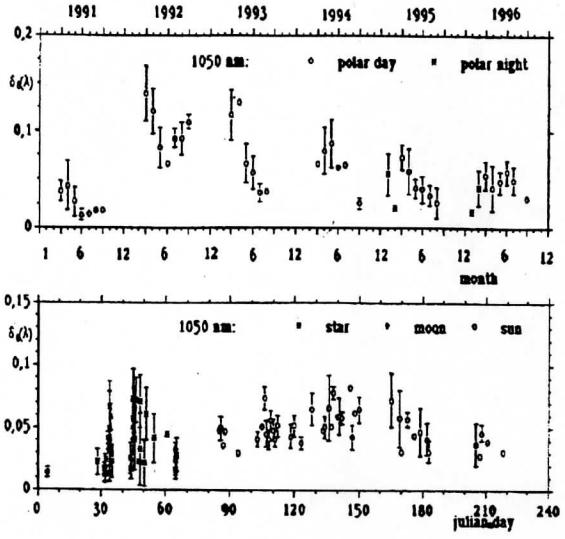

Figure 3: Optical depth at 1050 nm measured in arctic haze from Spitzbergen with a sun photometer, a moon photometer and a star photometer. The upper panel shows the monthly mean values from 1991 through 1996. The lower panel shows weekly mean values for 1996. (Herber et al. 1996)

Figure 4 suggests that the most "Diamond Dust" cases at the South Pole should produce GLAS altitude errors of less than 1 cm. However, Ohtake et al.(1982) report observations of large numbers of particles less than 50 microns in radius downwind of leads in the arctic ice pack and in ice fogs over Fairbanks, Alaska. These observations coupled with the lack of small particle measurements at the south pole indicate that additional study of "Diamond Dust" scattering errors in GLAS measurements is prudent. This caution appears particularly appropriate for arctic observations.

5 Arctic Haze

A persistent, wide-spread haze with an average optical depth of approximately 0.05 at a wavelength of 1 micron is observed in the arctic (Shaw, 1982, 1995; Herber et al. 1996). Observations showing the seasonal variation of the optical depth are shown in figures 3 and 5. An example of the vertical distribution of the haze is presented in figure 6. Arctic haze is believed to be caused by industrial sources in northern Asia and Europe. Similar industrial sources are absent in the southern hemisphere and the haze does not appear to occur in Antarctica. The literature surveyed by this author does not provide information on the optical depth of the haze over the Greenland ice cap.

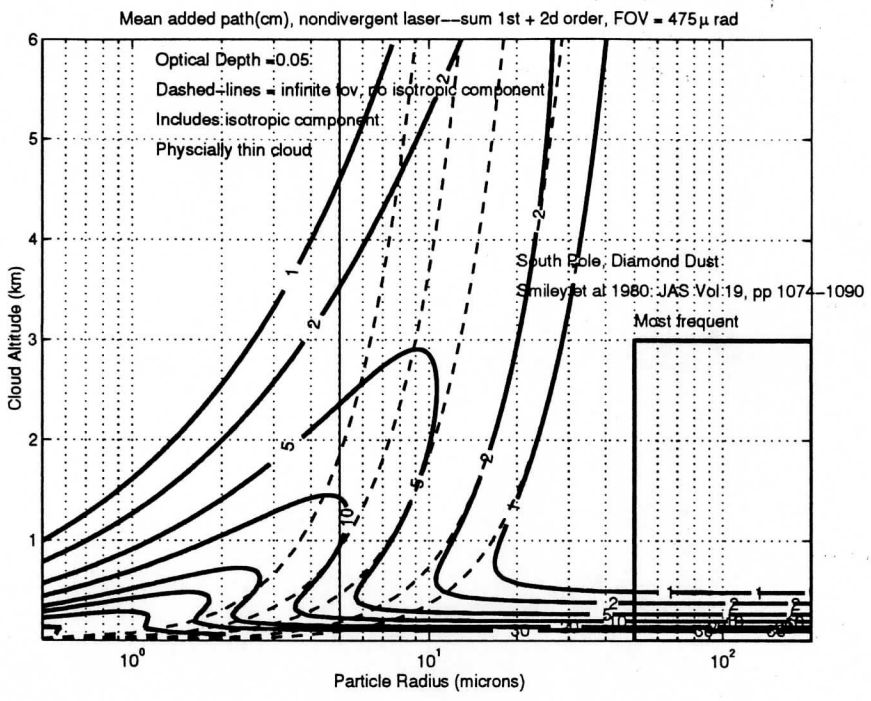

Figure 4: Average path delay for photons scattered from the earth's surface after passing through a physically thin "diamond dust" cloud with an optical depth of 0.05. Contours of constant path delay in centimeters are plotted as a function of cloud altitude and cloud particle radius (solid contours). The path delay contours are 1, 2, 5, 10, 20, 30 and 50 cm. Dashed lines show the average path delays for the Gaussian portion of the phase function in the case of an infinite receiver field of view. The bold box outlines altitudes and particles sizes which are most likely to occur during episodes of "diamond dust" ice crystal precipitation (Smiley et al., 1980). Particle sizes down to 5 microns (bold vertical line) were observed but not included in measured particle size distributions.

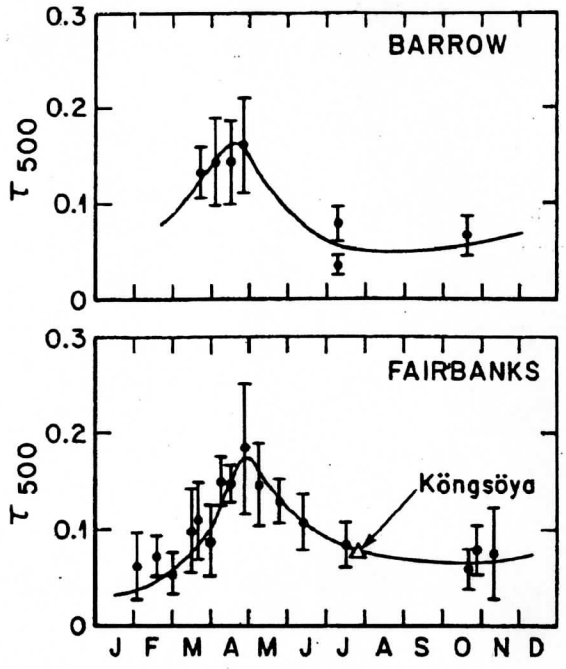

Figure 5: Annual variation of the optical depth in arctic haze measured at a wavelength of 500 nm (Shaw, 1982). Based on Shaw's measurement of the wavelength dependence of the scattering cross section these values should be multiplied by $2^{-1.7} = .31$ to estimate the 1 micron extinction cross section.

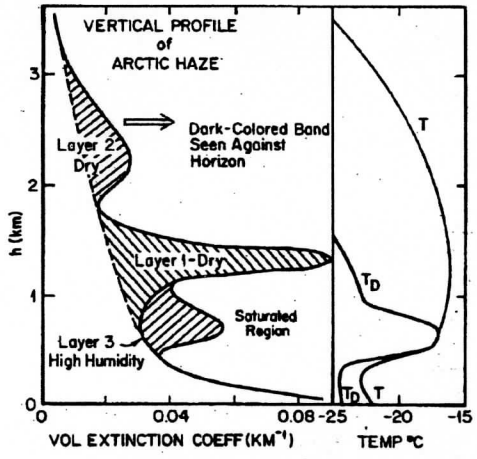

Figure 6: A vertical profile of the 500 nm extinction cross section measured at Barrow, Alaska in arctic haze (Shaw, 1982).

In order to estimate the potential altitude errors, we have used figure 3 to select 0.05 as a typical optical depth, and figure 6 to select altitudes of the haze and information from Shaw (1982) to estimate particle sizes. The estimated additional path is plotted in figure 7. This shows that dense haze layers near the ground can produce altitude errors greater than 10 cm. However, the available literature suggests that the haze normally consists of elevated layers such as shown in figure 6. Figure 7 suggests that the altitude errors produced by elevated arctic haze layers will normally be less than 1 cm. However, haze layers in the lowest 1 km may produce errors of 1 to 10 cm. As an added caution, the model we have used assumes particles which are large compared to the wavelength of the scattered light. This assumption is violated for the small end of the haze particle size distribution reported by Shaw (1982). In future models, a more careful approximation of the large angle portion the scattering phase function should replace the isotropic assumption used in equation 3.

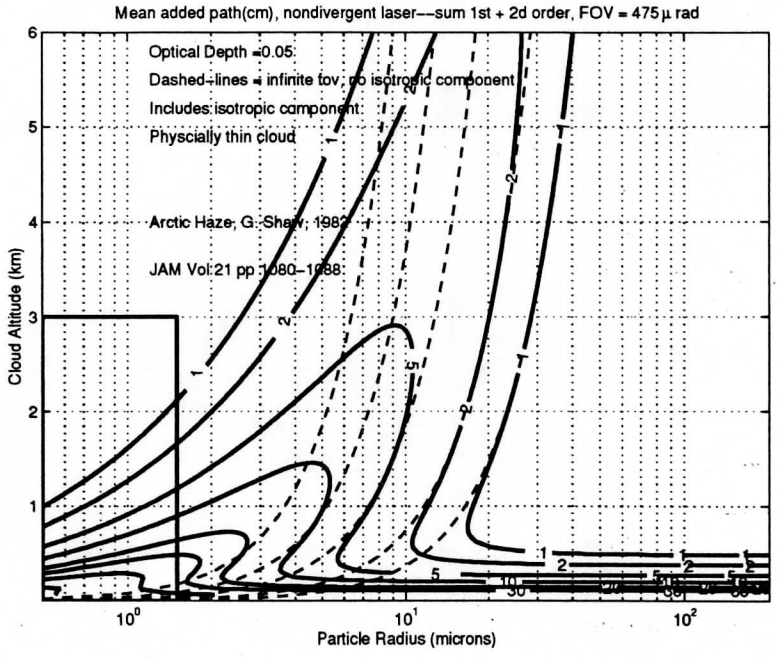

Figure 7: Average path delay for photons scattered from the earth's surface after passing through a physically thin arctic haze cloud with an optical depth of 0.05. Contours of constant path delay in centimeters are plotted as a function of cloud altitude and cloud particle radius (solid contours at 1, 2, 5 10 20 and 30 cm). Dashed lines show the average path delays for the Gaussian portion of the phase function in the case of an infinite receiver field of view. The bold box outlines altitudes and particles sizes which are likely to occur in arctic haze (Shaw, 1982).

6 Arctic Stratus

Surface cloud climatologies from the arctic indicate low altitude stratus cloud coverage is very prevalent. During winter, cloud coverages of 40% to 70% are recorded with sumer coverages as high as 90% reported (Curry et al., 1996). Much of the time these are water clouds with particles diameters $\sim$ 15 microns. Typical cloud bases are 1 km or less. Most clouds will be too dense for the lidar to penetrate. However, because so much of the arctic is covered with these clouds we expect that a large percentage of the lidar echos received from the surface will be obtained in regions near clouds or in holes between clouds. These areas are likely to contain tenuous cloud elements which will introduce scattering errors into the altitude measurements. To access the likely effect of arctic stratus on GLAS altitude measurements we have selected a very tenuous cloud with an optical depth, $\tau = 0.2$.

This might be found near arctic stratus decks or in holes between clouds. It is important to note that the optical depth of most arctic stratus is much larger than 0.2. Also, the GLAS altimeter will see surface reflections through clouds with $\tau \sim 1$ in which case the atmospheric scattering will contribute a much larger error. Because even the very tenuous cloud depicted in figure 8 can produce altitude errors of 20 to 30 cm, it is clear that GLAS altitudes obtained near arctic stratus are likely to contain significant biases. The literature examined in preparing this report contains little information on low altitude stratus cloudiness in Antarctica, however similar clouds are likely over low altitude portions of the continent and even the south pole shows a substantial fraction of overcast and broken cloud fields. Many of these cases may consist of low altitude clouds containing small particles which would produce large altitude errors.

Figure 9 shows that the path delays caused by atmospheric scattering can be dramatically reduced by decreasing the reciever field of view. This change also decreases the amount of background light collected by the receiver and thus improves the signal to noise ratio.

Figure 10 further illustrates the influence of receiver field-of-view on the bias errors produced by atmospheric scattering. This figure shows the average path delay generated by a physically thin arctic stratus cloud comprised of 10 micron diameter particles located at an altitude of 1 km. Path delays are plotted as a function of the cloud optical depth for the proposed 475μrad field of view and for a system where the field-of-view is reduced to 150μrad (note that 150μrad is the proposed field-of-view for the 532 nm cloud channel). When the the optical depth is greater than $\sim$ 0.5 m significant contributions to the average propagation delay will be caused by photons which are scattered more than once in the atmosphere. Thus, figure 10 will under estimate the path delay for optical depths greater than $\sim$ 0.5.

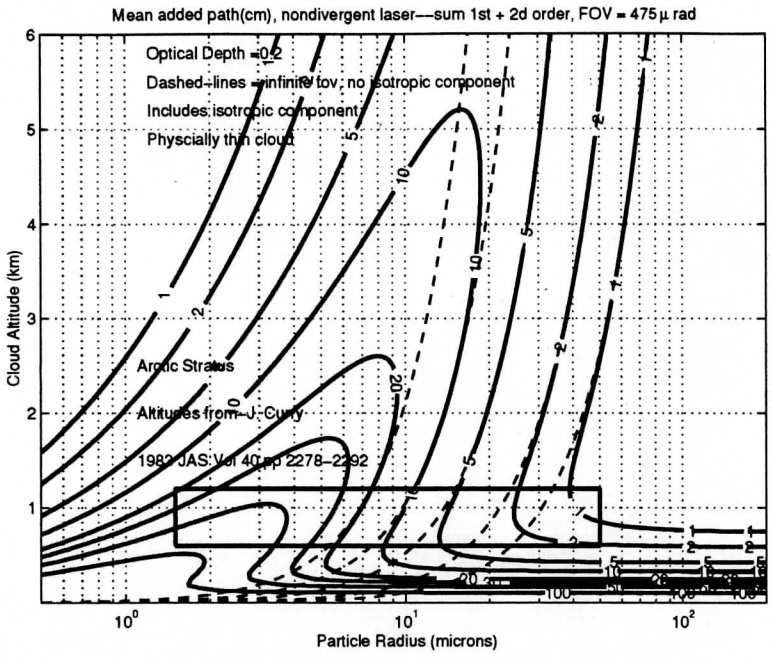

Figure 8: Average path delay for photons scattered from the earths surface after passing through a physically thin arctic stratus cloud with an optical depth of 0.2. Contours of constant path delay in centimeters are plotted as a function of cloud altitude and cloud particle radius (solid contours at 1 2 5 10 20 30 50 and 100 cm). Dashed lines show the average path delays for the Gaussian portion of the phase function in the case of an infinite receiver field of view. The bold box outlines altitudes and particles sizes which are likely to occur in arctic stratus clouds (Curry, 1983). The horizontal contour lines in the lower right depict contributions from the isotropic component of the phase function (eq. 3). These contributions become relatively important at low altitudes. Because the isotropic assumption is not a very good approximation to the large angle scattering by particles, future models must include an improved approximation to the phase function.

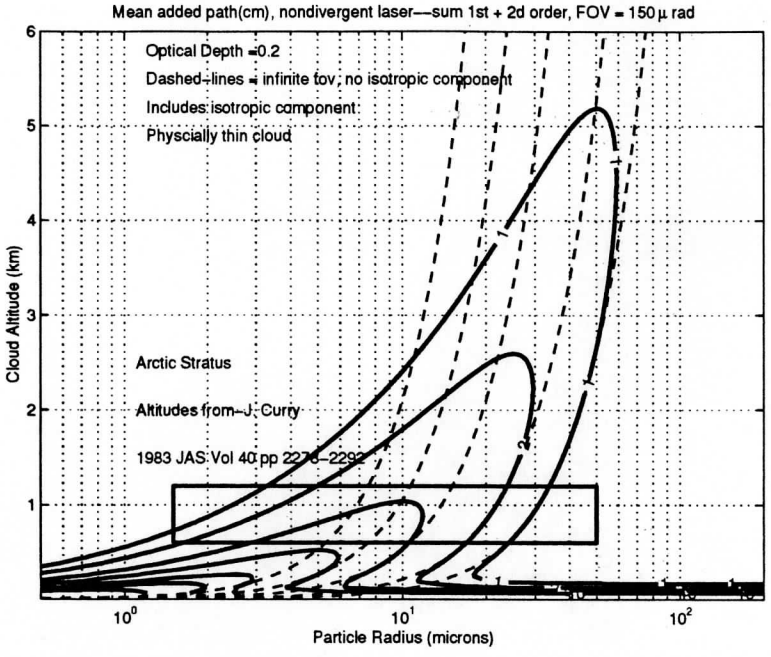

Figure 9: Average path delay for the conditions shown in figure 8 except that the the GLAS receiving telescope field of view has been decreased from 475 to 150μrad. Solid contours depicting path delays are plotted at 1, 2, 5, 10, 20, 30, and 50 cm). Notice the dramatic reduction of the average path delays relative to those presented in figure 8.

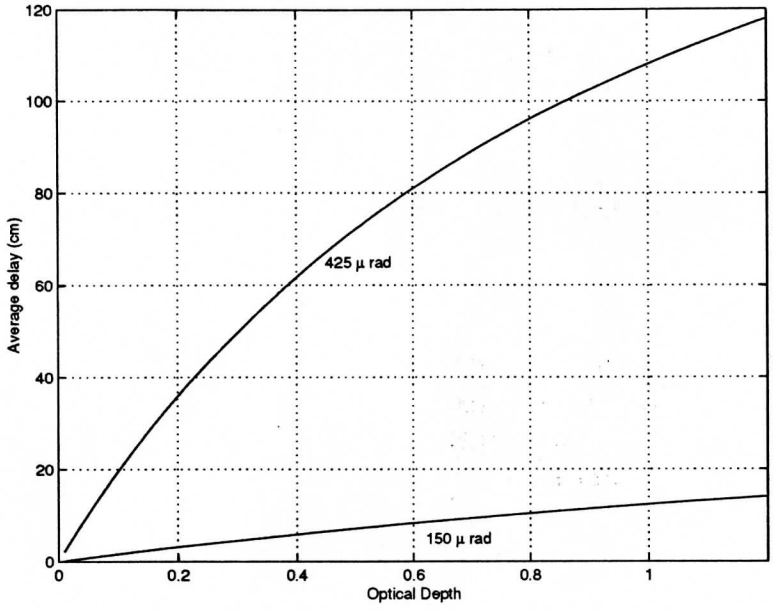

Figure 10: Average path delay as a function of optical depth for a physically thin arctic stratus cloud comprized of 5 micron radius droplets located at an altitude of 1 km. Path delays expected for a receiver field of view 475μrad are compared with those expected for a receiver field of view of 150μrad.

7 Conclusions

- Most GLAS lidar profiles will penetrate haze and/or clouds. Some of the detected photons will have been scattered by particles during the round trip to the surface. These scatterings will produce a bias in the measured altitudes.

- The contribution of atmospheric scattering to the lidar return is strongly dependent on the angular field of view of the receiving telescope. Reductions in the field of view could dramatically reduce the altitude bias resulting from atmospheric scattering.

- Even very tenuous arctic stratus will produce altitude errors of 20 cm and greater. Some climatologies suggest that $\sim$ 90% of summer days in the arctic have stratus clouds. GLAS measurements made in the vicinity of the stratus layers are likely to be significantly biased. Although not as well documented, similar clouds are likely to exist over Antarctica.

- The most common "Diamond Dust" conditions documented at the south pole appear to contain rather large ice crystals and rather small optical depths. These conditions will produce altitude biases of less than 1 cm. However, smaller ice crystal have been measured in other locations such as near open leads in ice packs and in the ice fogs which form over Fairbanks, Alaska. These conditions would cause larger errors. An additional caution results because the replicator used at the south pole could not measure small crystals. A large population of small crystals would increase the bias. Low altitude cirrus clouds consisting of very small ice crystals would also produce measurable altitude biases.

- Elevated layers of arctic haze conditions are likely to produce altitude errors of less than 1 cm. However, if the haze is confined below 1 km, errors in the range of 1 to 10 are possible. Scattering by the small end of the arctic haze particle size distribution may not be accurately described by the large particle approximations used in this treatment. This can be tested with monte Carlo simulations or by modifications in the above derivation, but this has not been completed at this time.

- Cloud cover over arctic and antarctic ice sheets is poorly known. GLAS will make a major contribution to our knowledge of high latitude cloudiness. This information is of great importance to the modeling of ice sheets and global climate.

8 References

- Benedetti, A., A. di Sarra, G. Fiocco, and D. Fua, 1996: Cirrus clouds at Thule, Greenland, during sumer: lidar observations and influence on the planetary radiative budget. *IRS '96: Current Problems in Atmospheric Radiation*, W. L. Smith and K. Stammes, Eds., A. Deepak, Hampton, VA., 23-26.

- Curry, J. A., 1983: On the formation of continental polar air. *J. Atmos. Sci.*, **40**, 2279-2292.

- Curry, J. A., 1996: Overview of arctic cloud and radiation characteristics, *J. Climate*, **9**, 1731-1764.

- Eloranta, E. W., 1998: A practical model for lidar multiple scattering. *Applied Optics*, **37**, 2464-2472.

- Herber, A. S. Debatin, J. Graeser, H. Gernandt, K. Schulz, A. Naebert, J. Gundermann, and G. Alekseeva, 1996: Measurements of the spectral optical depth of aerosols with moon and star light during polar night 1994/95 in Ny-Ålesund, Spitzbergen. *IRS '96: Current Problems in Atmospheric Radiation*, W. L. Smith and K. Stammes, Eds., A. Deepak, Hampton, VA., 19-22.

- Meyer, F. G., J. A. Curry, C. A. Brock, and L. F. Radke, 1991: Springtime visibility in the arctic. *J. of Appl. Meteor.*, **30**, 342-357.

- Ohtake, T., K. Jayaweera and K. Sakurai, 1982: Observation of ice crystal formation in lower arctic atmosphere. *J. Atmos. Sci.*, **39**, 2898-2904.

- Shaw, G. E., 1982: Atmospheric turbidity in the polar regions. *J. Appl. Meteor.*, **21**, 1080-1088.

- Shaw, G. E., 1995: The Arctic Haze Phenomena, *Bull. Am. Meteor. Soc.*, **76**, 2403-2412.

- Smiley, V. N., B. M. Whitcomb, B. M. Morley, and J. A. Warburton, 1980: Lidar determinations of atmospheric ice crystal layers at South Pole during clear-sky precipitation. *J. Appl. Meteor*, **19**, 1074-1090.

- Walden, V. P. and S. G. Warren, 1996: A spectral downward longwave climatology for clear and cloudy skies over South Pole, *IRS '96: Current Problems in Atmospheric Radiation*, W. L. Smith and K. Stammes, Eds., A. Deepak, Hampton, VA., 54-57.